

Chiral Topological Excitons in a Chern Band Insulator

Ke Chen^{1,2} and Ryuichi Shindou^{1,2,*}

¹International Center for Quantum Materials, Peking University, Beijing 100871, China

²Collaborative Innovation Center of Quantum Matter, Beijing 100871, China

(Dated: June 23, 2021)

A family of semiconductors called as Chern band insulator are shown to host exciton bands with non-zero topological Chern integers and chiral exciton edge modes. Using a prototypical two-band Chern insulator model, we calculate a cross-correlation function to obtain the exciton bands and their Chern integers. The lowest exciton band acquires Chern integers such as ± 1 and ± 2 in electronic Chern insulator phase. The non-trivial topology can be experimentally observed both by non-local optoelectronic response of exciton edge modes and by a phase shift in the cross-correlation response due to the bulk mode. Our result suggests that magnetically doped HgTe, InAs/GaSb quantum wells and (Bi,Sb)₂Te₃ thin film are promising candidates for a platform of topological excitonics.

Exciton is an electron-hole bound state in semiconductors, which plays central roles in semiconductor optoelectronics. A binding energy of the exciton becomes dramatically enhanced in low-dimensional semiconductors due to quantum confinement effect [1–3]. Well-studied examples are excitons in quantum dot [4–6], wire [7, 8], carbon nanotube [9–11] and two-dimensional materials such as transition metal dichalcogenide (TMDC) monolayer [12–28].

Topological excitonics in low-dimensional semiconductors [29–42] offers unique perspective in optoelectronics and future energy-harvesting materials. A topological exciton edge mode has an energy-momentum dispersion within the light cone and interacts with light (Fig. 1). Under p - n junction, such topological exciton edge modes enable strong electroluminescence (EL) with much longer exciton life time: the strong EL intensity is due to spatially localized nature of the edge exciton wavefunction and the longer life time can be associated with its limited decay process due to a peculiar topological protection of the modes. Unidirectional nature of topological chiral exciton edge modes enables novel *non-local* optoelectronic response. The first theoretical proposal was made in organic semiconductors [33, 34]. Thereby, dipolar interactions among Frenkel excitons play vital roles in realization of topological excitonics like in topological magnonics [43]. Synthetic gauge field in photon-exciton couplings endows polaritons with non-trivial band topology [35–37]. A bright exciton with a Dirac cone spectrum in TMDC monolayer [23, 38–40, 44] is theoretically suggested to realize topological exciton under Moiré patterns or moderate strains with external magnetic field [41, 42].

Chern insulator is a two-dimensional topological band insulator with broken time reversal symmetry in which the quantized Hall conductance is realized without external magnetic field [45]. The first material realization was proposed theoretically in magnetic atoms doped two-dimensional quantum spin Hall insulators [46–48]. Later, an experimental realization was achieved in a thin film of magnetic topological insulator, Cr-doped (Bi,Sb)₂Te₃ [49], where a magnetic field dependence of

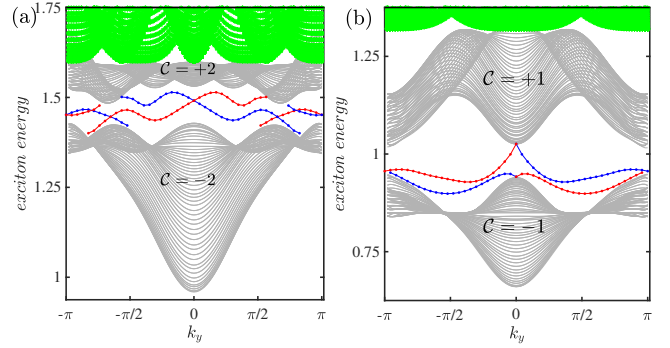


FIG. 1. (color online) Chiral exciton edge modes and exciton bulk modes (open/periodic boundary condition in x/y -axis). The blue and red line represent edge modes localized at opposite boundaries ($x = 0$ and $x = 30$ respectively). The green-color region is an electron-hole continuum due to transitions between bulk valence and conduction bands. (a) $U = 3.31, t' = 0.5, t = 1.5, m = 1$ (“ c ”-point in Fig. 3). (b) $U = 3.31, t' = 0.5, t = 1.16, m = 0.8$ (“ d ”-point in Fig. 3).

the two-dimensional Hall conductance clearly shows the quantized Hall conductance of $\pm e^2/h$ in the zero external field.

In this paper, we demonstrate that the Chern band insulator provides unprecedented opportunity to explore rich topological exciton physics. We show that a prototypical model for the Chern band insulator hosts exciton bands with non-zero topological integers and topological chiral exciton edge modes that are bright. We study a two-band square lattice model for the Chern band insulator with an inclusion of on-site Coulomb repulsion term, to calculate a linear response function among density and pseudospin degree of freedoms. Eigenvalues of the matrix-formed response function have a well-defined pole below electron-hole continuum, which describes an energy-momentum dispersion for exciton excitations in the Chern insulator. We define topological Chern integer for the exciton bands from the corresponding eigenvectors. We reveal that the lowest and second lowest exciton bands acquire a variety of non-zero Chern inte-

gers within a parameter region for the Chern insulator phase. Consequently, the integer number of chiral exciton modes localized in boundaries run across the band gap between these exciton bulk bands. From their wavefunctions and dispersions, they are bright excitons. We argue that the non-trivial band topology of the exciton bulk bands can be directly mapped out by a measurement of a phase shift of the cross-correlation encoded in the matrix-formed response function.

The model.— The first material realization of Chern band insulator is proposed in Mn atoms doped two-dimensional quantum spin Hall systems such as HgTe and InAs/GaSb quantum wells [46–48]. When ferromagnetically ordered (magnetic moment upward), the doping magnetic atoms induce exchange fields both in conduction electron band (*s*-wave band) and hole band (*p*-wave band) but in an opposite direction with each other, which renders a band inversion between the electron band with down spin (\downarrow) and the hole band with up spin (\uparrow) to be reinverted, while leaving intact the band inversion between the other pair. This leads to a low-energy effective two-band model for the Chern insulator [50]. In the momentum space, $\mathbf{k} \equiv (k_x, k_y)$, the kinetic energy part of the Hamiltonian on square lattice takes a form of $\mathcal{H}_0 \equiv \sum_{\mathbf{k}} \mathbf{c}_{\mathbf{k}}^\dagger \mathbf{H}_{sp}(\mathbf{k}) \mathbf{c}_{\mathbf{k}}$ with

$$\mathbf{H}_{sp}(\mathbf{k}) \equiv -t' (\cos k_x + \cos k_y) \boldsymbol{\sigma}_0 + \sin k_x \boldsymbol{\sigma}_1 + \sin k_y \boldsymbol{\sigma}_2 + (m - t (\cos k_x + \cos k_y)) \boldsymbol{\sigma}_3 \quad (1)$$

and $\mathbf{c}_{\mathbf{k}}^\dagger \equiv (c_{\mathbf{k},s,\uparrow}^\dagger, c_{\mathbf{k},p,\downarrow}^\dagger)$. $\boldsymbol{\sigma}_a$ is a 2×2 Pauli matrix composed by *s* orbital with \uparrow and $p_+ \equiv p_x + ip_y$ orbital with \downarrow . $-t - t'$ (< 0) and $t - t'$ (> 0) are the nearest neighbor intra-orbital hopping integrals for *s* and p_+ orbitals respectively. m is an atomic energy difference between the two orbitals. For $|m| < |2t|$, an inter-orbital hopping due to the relativistic spin-orbit interaction induces a band gap, making the system to be QAH insulator (Chern insulator) [50]. The inter-orbital hopping with odd spatial parity dictates that uniform electric currents J_x and J_y contain pseudospin density components: $J_\mu = \sum_{\mathbf{k}} \mathbf{c}_{\mathbf{k}}^\dagger \cos k_\mu \boldsymbol{\sigma}_\mu \mathbf{c}_{\mathbf{k}} + \dots$ ($\mu = x(1), y(2)$). We take the inter-orbital hopping to be unit. As for a screened Coulomb interaction, we consider an on-site Coulomb interaction $U (> 0)$ for simplicity:

$$\mathcal{V} = \frac{1}{2} \frac{U}{N^2} \sum_{\mathbf{k}_1, \mathbf{k}_2, \mathbf{q}, \alpha, \beta} c_{\mathbf{k}_1 + \mathbf{q}, \alpha}^\dagger c_{\mathbf{k}_2 - \mathbf{q}, \beta}^\dagger c_{\mathbf{k}_2, \beta} c_{\mathbf{k}_1, \alpha} \quad (2)$$

with $\alpha, \beta = 1, 2$ which stand for (*s*, \uparrow) and (*p*, \downarrow) respectively. N^2 is total number of the square lattice sites.

Response function and Topological integer.— The Chern integer for exciton bulk band is a central building block of topological excitonics. We define this in connection with linear response of the system against external perturbations. Consider an external field $\mathbf{J}_b(\mathbf{r}_m)$ which couples with the density ($a = 0$) and pseudospin degree of freedom ($a = 1, 2, 3$): $\mathcal{O}_a(\mathbf{r}_j) \equiv$

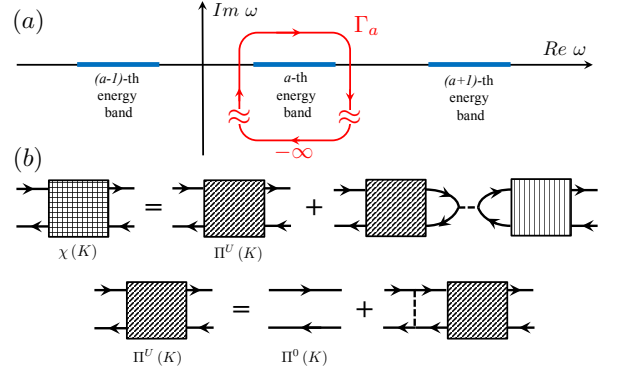


FIG. 2. (color online) (a) Closed loop along which an integral over complex ω is taken in Eq. (3). (b) Feynman diagrams for the correlation function within the generalized random phase approximation. Π^U : two-particle irreducible Green's function, Π^0 : bare polarization part.

$c_{\mathbf{r}_j, \alpha}^\dagger (\boldsymbol{\sigma}_a)_{\alpha\beta} c_{\mathbf{r}_j, \beta}$. The density and pseudospin densities induced by the external fields are given by a linear response function as $\langle \mathcal{O}_a(\mathbf{r}_j, t) \rangle = \int d\mathbf{r}_m \int_{-\infty}^{\infty} dt' \chi_{ab}^R(\mathbf{r}_j - \mathbf{r}_m, t - t') \mathbf{J}_b(\mathbf{r}_m, t')$ with $\chi_{ab}^R(\mathbf{r}_j - \mathbf{r}_m, t - t') \equiv -i\theta(t - t') \langle [\mathcal{O}_{a,H}(\mathbf{r}_j, t), \mathcal{O}_{b,H}(\mathbf{r}_m, t')] \rangle$. The response function in the dual space, $\chi_{ab}^R(\mathbf{k}, \omega) \equiv \int dt d\mathbf{r} e^{-i\mathbf{k}\cdot\mathbf{r} + i\omega t} \chi_{ab}^R(\mathbf{r}, t)$, is directly related to the optical conductivity in some cases. For example, when bright excitons are composed mainly by particle-hole pairs near the time-reversal symmetric momentum points, χ_{11}^R , χ_{12}^R and χ_{22}^R associated with these excitons (divided by frequency ω) contribute directly to optical conductivities, σ_{xx} , σ_{xy} and σ_{yy} respectively.

From an analogy of the quantum Hall physics [51–54], the Chern integer for the *a*-th bulk exciton band (*a* is an index for the bulk band) is defined by the response function in the dual space:

$$C_a \equiv \frac{\epsilon_{\mu\nu}}{2} \int_{\text{BZ}} \frac{d\mathbf{k}}{2\pi} \oint_{\Gamma_a} \frac{d\omega}{2\pi} \text{Tr} \left[\frac{\partial \chi^R}{\partial \omega} \frac{\partial (\chi^R)^{-1}}{\partial k_\mu} \chi^R \frac{\partial (\chi^R)^{-1}}{\partial k_\nu} \right], \quad (3)$$

Here an integral over ω is along a loop Γ_a which encompasses an energy region of the *a*-th bulk band on the real ω axis (Fig. 2). In the dilute electron and hole density limit [55–57], the response function can be calculated by a generalized random phase approximation (Fig. 2),

$$\chi_{ab}^R(\mathbf{k}, \omega) = \chi_{ab}^T(\mathbf{k}, i\omega_n = \omega + i\eta), \quad (4)$$

$$\chi_{ab}^T(K) = \Pi_{ab}^U(K) + \frac{U \Pi_{a0}^U(K) \Pi_{0b}^U(K)}{1 - U \Pi_{00}^U(K)}, \quad (5)$$

$$\Pi^U(K) = \Pi^0(K) \left[\mathbf{1}_{4 \times 4} + \frac{U}{2} \Pi^0(K) \right]^{-1}, \quad (6)$$

$$\Pi_{ab}^0(K) \equiv \frac{1}{\beta} \frac{1}{N^2} \sum_Q \text{Tr} [\boldsymbol{\sigma}_a \mathbf{g}^0(Q + K) \boldsymbol{\sigma}_b \mathbf{g}^0(Q)], \quad (7)$$

with $K \equiv (\mathbf{k}, i\omega_n)$ and $Q \equiv (\mathbf{q}, i\epsilon_n)$. A 2×2 bare electron Green's function $\mathbf{g}^0(Q)$ is given by eigenvectors of

$\mathbf{H}_{sp}(\mathbf{q}), |\mathbf{q}, j\rangle$:

$$\mathbf{g}^0(\mathbf{q}, i\epsilon_n) \equiv \sum_{j=c,v} \frac{|\mathbf{q}, j\rangle\langle\mathbf{q}, j|}{i\epsilon_n - \mathcal{E}_{\mathbf{q},j} + \mu}$$

with $\mathbf{H}_{sp}(\mathbf{q})|\mathbf{q}, j\rangle = \mathcal{E}_{\mathbf{q},j}|\mathbf{q}, j\rangle$. $j = c, v$ denotes conduction and valence band respectively. Recast in the picture of effective single-exciton Hamiltonian [58, 59], the first term in Eq. (5) (ladder diagrams) corresponds to the direct interaction between electron and hole, while the second term corresponds to the exchange interaction. For simplicity of the calculation, we have considered only the ladder diagrams.

Below the electron-hole continuum, $\omega < \min_{\mathbf{q}}(\mathcal{E}_{\mathbf{q}+\mathbf{k},c} - \mathcal{E}_{\mathbf{q},v})$, the response function $\chi^R(\mathbf{k}, \omega)$ is Hermitian and is diagonalized by a unitary matrix, unless one of its eigenvalues has a pole. Namely,

$$[\chi^R(\mathbf{k}, \omega)]^{-1} |u_a(\mathbf{k}, \omega)\rangle = |u_a(\mathbf{k}, \omega)\rangle L_a(\mathbf{k}, \omega),$$

where $|u_a(\mathbf{k}, \omega)\rangle$ with $a = 0, 1, 2, 3$ form an orthonormal basis for those ω with $L_a(\mathbf{k}, \omega) \neq 0$ for all a . The eigenvalue has at most one pole for each a in the energy region below the electron-hole continuum, $\omega = E_{a,\mathbf{k}}$ with $L_a(\mathbf{k}, E_{a,\mathbf{k}}) = 0$, which determines an energy-momentum dispersion of the a -th exciton bulk band. Near each pole, the response function takes an asymptotic form

$$\chi^R(\mathbf{k}, \omega) = |\tilde{u}_a(\mathbf{k})\rangle \frac{A_a(\mathbf{k})}{\omega - E_{a,\mathbf{k}} + i\eta} \langle\tilde{u}_a(\mathbf{k})| + \dots \quad (8)$$

$|\tilde{u}_a(\mathbf{k})\rangle \equiv |u_a(\mathbf{k}, E_{a,\mathbf{k}})\rangle$ is a Bloch wavefunction for the a -th bulk exciton band and $A_a^{-1}(\mathbf{k}) \equiv \frac{\partial L_a}{\partial \omega}|_{\omega=E_{a,\mathbf{k}}}$ is the inverse of a spectral weight. Eqs. (3,8) give the Chern integer in terms of the Berry curvature defined by the Bloch wavefunction $|\tilde{u}_a\rangle$: $C_a \equiv \frac{1}{\pi} \int d\mathbf{k} \text{Im}(\partial_{k_y} \langle\tilde{u}_a|) (\partial_{k_x} |\tilde{u}_a\rangle)$ [60, 61].

Phase diagram.— For moderately large U ($2 \lesssim U \lesssim 5$), the lowest and second lowest exciton bands are well separated from the electron-hole continuum. Such exciton bands almost always take a variety of non-zero Chern integers in the Chern insulator phase region ($|m| < 2|t|$). Fig. 3 shows a distribution of the Chern integer of the lowest exciton band around $U = 3$ and 4. When the integer changes from one to another, the two exciton bands form a linear or quadratic band touching. The transitions from +2 to 0 (labelled in Fig. 3(a)), from 0 to -2, and from -2 to -1 region are accompanied by a quadratic band touching at Γ point, linear touching at two M points, $\mathbf{k} = (0, \pi)$, $(\pi, 0)$, and linear touching at P point, $\mathbf{k} = (\pi, \pi)$, respectively.

Effective 2×2 Hamiltonians for these exciton band touchings can be derived from a symmetry argument of a Bethe-Salpeter (BS) Hamiltonian for single exciton wavefunction [63]. The BS Hamiltonian is symmetric under a magnetic point group $4m'm'$. The eigen wavefunctions of the BS Hamiltonian at Γ and P point form an irreducible

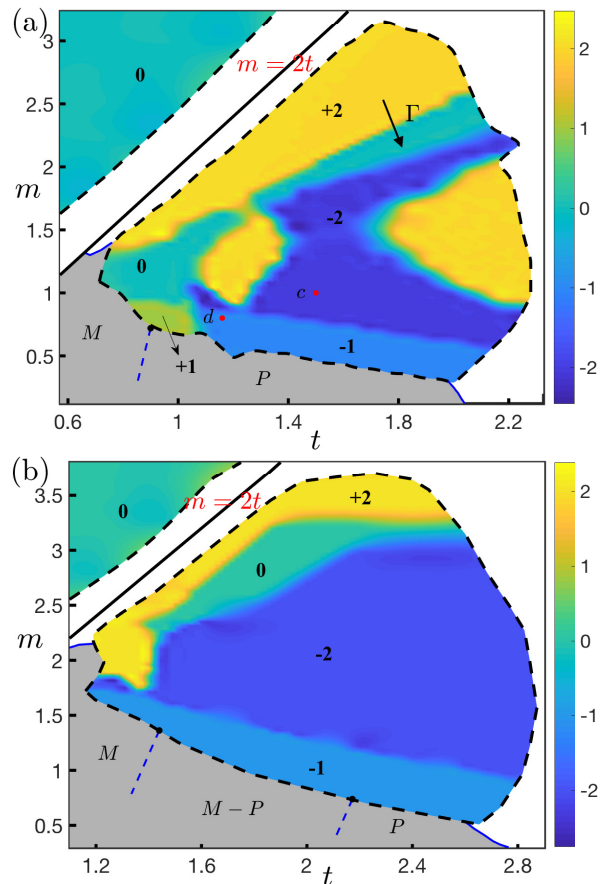


FIG. 3. (color online) Distributions of the Chern integer of the lowest exciton bulk band in (t, m) parameter space at $U = 3.31, t' = 0.5$ (a) and at $U = 3.95, t' = 1.0$ (b). Regions with colors (yellow, green, blue, yellow green, light blue) and with Chern integers (+2, 0, -2, +1, -1) represent those parameter regions where the lowest exciton bulk band is well separated from the electron-hole continuum in the whole Brillouin zone (BZ). In the white region, the band enters the continuum at certain points of the BZ. When the parameters are tuned from the colored regions to the grey region, the lowest exciton band touches the zero energy, giving rise to an exciton condensation. The labels ‘ M ’, ‘ P ’ and ‘ $M - P$ ’ indicate that the exciton condensation occurs at the M , P , and points between M and P point respectively.

corepresentation (IcREP) of $4m'm'$. There are four distinct 1-dimensional IcREPs of $4m'm'$ under which the eigen wavefunction has s , d , $p_x + ip_y$ and $p_x - ip_y$ -wave symmetry respectively. The exciton band touchings are composed by two states belonging to distinct IcREPs. An analysis shows that the quadratic band touching at Γ point is composed by two odd-parity states (p_+ and p_-) or two even-parity states (s and d) [63]. The linear band touching at P point is by even and odd states (e.g. s and p_+).

For the ordinary insulator region ($|m| > 2|t|$), we observe only single exciton bulk band with zero Chern integer below the electron-hole continuum: being consistent

with an ionic limit ($m \gg 2t$), where the BS Hamiltonian is completely real-valued. When U gets much larger than the band gap (e.g. $U \gtrsim 5$), the lowest exciton bulk band reaches the zero energy at high symmetric points such as M and P points, only to exhibit an exciton condensation (Fig. 3). The resulting electronic phase for $|m| < 2|t|$ is another band insulator with reduced translational symmetry.

Nature of topological chiral exciton edge modes.— In the region with non-zero Chern integers in Fig. 3, the response function is calculated for the system with open boundary condition in one direction (x) and periodic condition in the other (y): $\chi_{ab}^R(x_j, x_m; k_y, \omega)$ with k_y momentum conjugate to y [63]. When an indirect gap opens between the lowest two exciton bulk bands, the response function acquires several new poles inside the gap. The poles give chiral dispersions as a function of k_y , connecting the two exciton bulk bands (Fig. 1). We observe that the number of chiral dispersions with sign (+ for left and – for right-handed) is consistently identical to Chern integer of the lowest exciton band \mathbb{Z} [64, 65]. The eigen wavefunctions of the response function which correspond to these new poles are all localized at the spatial boundaries. They have significant weights in the pseudospin components of σ_1 and σ_2 , representing chiral exciton edge modes that interact with light.

The Chern band insulator has a gapless electronic edge mode with right and left-handed chiral dispersion for $0 < m < 2t$ and $-2t < m < 0$ respectively [50]. In low-energy region, electron-hole excitations along the electronic edge mode form an 1-dimensional collective excitation (chiral phason mode) [66], which can have level crossings with low-energy exciton edge modes. Being not protected by symmetry, the crossings lead to level repulsions (Fig. 4). Thus, total number of chiral dispersions of the *low-energy* edge excitons inside the indirect gap becomes $\mathbb{Z}-1$ for $0 < m < 2t$ and $\mathbb{Z}+1$ for $-2t < m < 0$ instead of \mathbb{Z} (\mathbb{Z} also changes sign under $m \rightarrow -m$). In high-energy region (lower than the electron-hole continuum associated with the bulk states), the electron-hole excitations along the edge provide another continuum due to finite curvature of the electronic edge mode dispersion. This edge electron-hole continuum gives a finite life time to the chiral exciton edge modes, when they share energy and momentum (Fig. 4).

Phase shift in the cross response function.— When the exciton bulk band has a non-zero Chern integer, $C_a \neq 0$, there always exists a momentum $\mathbf{k}_{0,j}$ in the BZ at which $\langle j|\tilde{u}_a\rangle = 0$ and around which the component has a $U(1)$ phase winding $\langle j|\tilde{u}_a\rangle \propto e^{i\theta_{\mathbf{k},j}}$ with $\oint_{|\mathbf{k}-\mathbf{k}_{0,j}|=\epsilon} \nabla_{\mathbf{k}} \theta_{\mathbf{k},j} \cdot d\mathbf{k} = \mathbb{Z}$ for any $j = 0, 1, 2, 3$ [51, 52]. The phase winding can be directly mapped out by a phase-sensitive spectroscopic measurement of χ^R , e.g., a phase-sensitive Brillouin light scattering [67–69]. Thereby, an incident probe light wave excites exciton at a -th bulk band with mo-

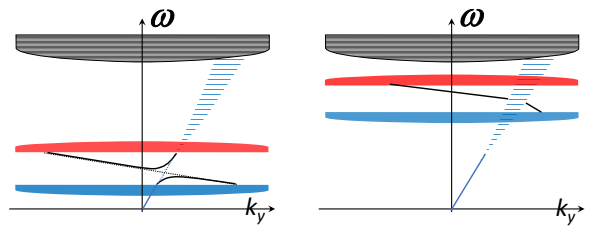


FIG. 4. (color online) Schematic pictures of level repulsion between chiral phason mode and exciton edge mode (left), and chiral exciton edge mode decaying in edge electron-hole continuum (right). Electron-hole excitations along the gapless chiral electronic edge mode form the chiral phason mode (blue solid line) in low-energy region and edge electron-hole continuum (blue shaded region) in high-energy region. Black solid line, black shaded region, blue region and red region stand for chiral exciton edge mode, bulk electron-hole continuum, the lowest and 2nd lowest exciton bulk bands respectively.

mentum \mathbf{k} , which leads to an absorption at $\omega = E_{a,\mathbf{k}}$. Eq. (8) dictates that the absorption spectrum in the cross-correlation component $\chi_{jl}^R(\mathbf{k}, \omega = E_{a,\mathbf{k}})$ ($j \neq l$) acquires a phase shift of $\Delta\theta_{\mathbf{k}} \equiv \theta_{\mathbf{k},j} - \theta_{\mathbf{k},l}$ with $\langle l|\tilde{u}_a\rangle \propto e^{i\theta_{\mathbf{k},l}}$. When \mathbf{k} goes around the boundary of an area S in the \mathbf{k} space that encloses $\mathbf{k}_{0,j}$, the phase shift shows a $U(1)$ phase holonomy of $2\pi\mathbb{Z}$. The phase holonomy is determined only by the number of the vortex of $\theta_{\mathbf{k},j}$ within the area S minus that of $\theta_{\mathbf{k},l}$.

Conclusion.— A prototypical Chern insulator model with an on-site Coulomb interaction hosts exciton bands with non-zero topological Chern integers such as ± 1 and ± 2 in the Chern insulator phase, with consequent chiral exciton edge modes. The chiral exciton edge mode may have level repulsion with chiral edge phason mode in low energy region, while short-wavelength exciton edge mode can be damped into edge electron-hole excitations only in a small region of its wavelength. The non-trivial band topology can also be observed from a phase shift in the cross-correlation response by a phase-sensitive spectroscopic measurement. The Chern insulator in magnetic topological insulator thin film [49, 70] can be described by the same low-energy effective continuous model of Eq. (1) [71], therefore can host qualitatively similar chiral topological excitons as in this paper. Our results also suggest that other quantum anomalous Hall insulators such as ferromagnetic graphene under YIG [72] are also potential candidates for seeking topological excitons.

The authors thank Junren Shi for helpful discussions. This work was supported by NBRP of China Grants No. 2014CB920901, No. 2015CB921104, and No. 2017A040215.

* rshindou@pku.edu.cn

- [1] L. V. Keldysh, JETP Lett. **29**, 658 (1979).
- [2] Al. L. Efros, and A. L. Efros, Sov. Phys. Semicond. **16**, 772 (1982).
- [3] L. Brus, J. Chem. Phys. **79**, 5566 (1983).
- [4] A. I. Ekimov, Al. L. Efros, and A. A. Onushchenko, Solid State Commun. **56**, 9221 (1985).
- [5] AL. Efros, M. Rosen, M. Kuno, M. Nirmal, D. J. Norris, M. Bawendi, Phys Rev. B **54**, 4843 (1996).
- [6] D. J. Norris, M. G. Bawendi, Phys. Rev. B **53**, 16338 (1996).
- [7] Y. Arakawa, and H. Sakaki, Appl. Phys. Lett. **40**, 939 (1982).
- [8] M. Asada, Y. Miyamoto, and Y. Suematsu, IEEE, J. Quantum Electron. **QE-22**, 1915 (1986).
- [9] F. Wang, G. Dukovic, L. E. Brus, and T. F. Heinz, Science **308**, 838 (2005).
- [10] J. Maultzsch, et. al. Phys. Rev. B **72**, 241402(R) (2005).
- [11] M. S. Dresselhaus, G. Dresselhaus, R. Saito, and A. Jorio, Annu. Rev. Phys. Chem. **58**, 719 (2007).
- [12] J. Feng, X. Qian, C. W. Huang, and J. Li, Nature Photonics **6**, 866 (2012).
- [13] T. Cheiwchanchamnangij, and W. R. L. Lambrecht, Phys. Rev. B **85**, 205302 (2012).
- [14] A. Ramasubramaniam, Phys. Rev. B **86**, 115409 (2012).
- [15] H. P. Komsa, and A. Krasheninnikov, Phys. Rev. B **86**, 241201(R) (2012).
- [16] H. L. Shi, H. Pan, Y. W. Zhang, and B. I. Yakobson, Phys. Rev. B **87**, 155304 (2013).
- [17] D. Y. Qiu, F. H. da Jornada, and S. G. Louie, Phys. Rev. Lett. **111**, 216805 (2013).
- [18] X. Xu, W. Yao, D. Xiao, and T. F. Heinz, Nature Phys. **10**, 343 (2014).
- [19] H Zeng, J Dai, W Yao, D Xiao, X Cui, Nature Nanotechnology **7**, 490 (2012).
- [20] D. Lagarde, L. Bouet, X. Marie, C. R. Zhu, B. L. Liu, T. Amand, P. H. Tan, and B. Urbaszek, Phys. Rev. Lett. **112**, 047401 (2014).
- [21] C. Mai, A. Barrette, Y. Yu, Y. G. Semenov, K. W. Kim, L. Cao, and K. Gundogdu, Nano Lett. **14**, 202 (2014).
- [22] Q. Wang, S. Ge, X. Li, J. Qiu, Y. Ji, J. Feng, and D. Sun, ACS Nano **7**, 11087 (2013).
- [23] T. Yu and M. W. Wu, Phys. Rev. B **89**, 205303 (2014).
- [24] T. Cao, G. Wang, W. Han, H. Ye, C. Zhu, J. R. Shi, Q. Niu, P. Tan, E. G. Wang, B. Liu and J. Feng, Nature Comm. **3**, 887 (2012).
- [25] A. M. Jones, H. Yu. N. J. Ghimire, S. Wu. G. Aivazian, J. S. Ross, B. Zhao, J. Yan, D. G. Mandrus, D. Xiao, W. Yao, and X. Xu, Nature Nanotechnology, **8**, 634 (2013).
- [26] A. Pospischil, M. M. Furchi, and T. Muller, Nature Nano. **9**, 257 (2014).
- [27] B. W. Baugher, H. O. H. Churchill, Y. Yang, P. Jarillo-Herrero, Nature Nano. **9**, 262 (2014).
- [28] J. S. Ross, P. Klement, A. M. Jones, Nirmal J. Ghimire, J. Yan, D. J. Mandrus, T. Taniguchi, K. Watanabe, K. Kitamura, W. Yao, D. H. Cobden, and X. Xu, Nature Nano. **9**, 268 (2014).
- [29] G. J. Sreejith, A. Wójs, and J. K. Jain, Phys. Rev. Lett. **107**, 136802 (2011).
- [30] B. Seradjeh, J. E. Moore, and M. Franz, Phys. Rev. Lett. **103**, 066402 (2009).
- [31] B. Seradjeh, Phys. Rev. B **85**, 235146 (2012).
- [32] J. Budich, B. Trauzettel, and P. Michetti, Phys. Rev. Lett. **112**, 146405 (2014).
- [33] J. Yuen-Zhou, S. K. Saikin, N. Y. Yao, Aln Aspuru-Guzik, Nat. Mater. **13** 10026 (2014).
- [34] J. Yuen-Zhou, S. K. Saikin, T. Zhu, M. C. Onbasli, C. A. Ross, V. Bulovic, and M. A. Baldo, Nat. Commun. **7**, 11783 (2016).
- [35] T. Karzig, C.-E. Bardyn, N. H. Lindner, and G. Refael, Phys. Rev. X **5**, 031001 (2015).
- [36] A. V. Nalitov, D. D. Solnyshkov, and G. Malpuech, Phys. Rev. Lett. **114**, 116401 (2015).
- [37] C. E. Bardyn, T. Karzig, G. Refael, and T. C. H. Liew, Phys. Rev. B **91**, 161413 (2015).
- [38] H. Yu, G. B. Liu, P. Gong, X. Xu, and W. Yao, Nature Comm. **5**, 3876 (2014).
- [39] H. Yu, X. Cui, X. Xu, and W. Yao, Natl. Sci. Rev. **2**, 57 (2015).
- [40] F. Wu, F. Qu, and A. H. MacDonald, Phys. Rev. B **91**, 075310 (2015).
- [41] F. Wu, T. Lovorn, and A. H. MacDonald, Phys. Rev. Lett. **118**, 147401 (2017).
- [42] Z. R. Gong, W. Z. Luo, Z. F. Jiang, and H. C. Fu, Scientific Reports, **7**, 42390 (2017).
- [43] R. Shindou, R. Matsumoto, S. Murakami, and J-i. Ohe, Phys. Rev. B **87**, 174427 (2013); R. Shindou, J-i. Ohe, R. Matsumoto, S. Murakami, E. Saitoh, Phys. Rev. B **87**, 174402 (2013); R. Shindou, and J-i. Ohe, Phys. Rev. B **89**, 054412 (2014); B. Xu, T. Ohtsuki, and R. Shindou, Phys. Rev. B **94**, 220403(R) (2016).
- [44] J. Zhou, W. Y. Shan, W. Yao, and D. Xiao, Phys. Rev. Lett. **115**, 116803 (2015).
- [45] F. D. M. Haldane, Phys. Rev. Lett. **61**, 2015 (1988).
- [46] C. X. Liu, X. L. Qi, X. Dai, Z. Fang, S. C. Zhang, Phys. Rev. Lett. **101**, 146802 (2008).
- [47] Q.-Z. Wang, X. Liu, H.-J. Zhang, N. Samarth, S.-C. Zhang, and C.-X. Liu, Phys. Rev. Lett. **113**, 147201 (2014).
- [48] C. X. Liu, S.-C. Zhang, and X.-L. Qi, Annu. Rev. Condens. Matter Phys. **7**, (2016).
- [49] C. Z. Chang, et. al. Science, **340**, 167 (2013).
- [50] X. L. Qi, Y. S. Wu, S. C. Zhang, Phys. Rev. B **74**, 085308 (2006).
- [51] D. J. Thouless, M. Kohmoto, M. P. Nightingale, and M. den Nijs, Phys. Rev. Lett. **49**, 405 (1982).
- [52] M. Kohmoto, Annals of Physics, **160** 343 (1985).
- [53] K. Ishikawa, and T. Matsuyama, Nucl. Phys. B **280**, 523 (1987).
- [54] K. Ishikawa, and T. Matsuyama, Zeitschrift fur Physik C **33**, 41 (1986).
- [55] A. L. Fetter and J. D. Walecka, *Quantum Theory of Many-Particle Systems* (Dover Publications, Mineola, New York, 2003), Chap. 4, p. 128.
- [56] W. Hanke and L. J. Sham, Phys. Rev. B **21**, 4656 (1980).
- [57] S. Maiti, V. A. Zyuzin, and D. L. Maslov, Phys. Rev. B **91**, 035106 (2015).
- [58] G. E. Pikus and G. L. Bir, Zh. Eksp. Teor. Fiz. **60**, 195 (1971) [Sov. Phys. JETP **33**, 108 (1973)].
- [59] M. Z. Maialle, E. A. de Andrada e Silva, and L. J. Sham, Phys. Rev. B **47**, 15776 (1993).
- [60] F. D. M. Haldane, Phys. Rev. Lett. **93**, 206602 (2004).
- [61] R. Shindou and L. Balents, Phys. Rev. Lett. **97**, 216601 (2006); Phys. Rev. B **77**, 035110 (2008).
- [62] C. J. Bradley, and A. P. Cracknell, *The Mathematical Theory of Symmetry in Solids* (The Clarendon Press, Oxford, 1972). Chap. 7, p. 569.
- [63] See Supplemental Material for the symmetry analysis on the Bethe-Salpeter Hamiltonian, calculation of the re-

sponse function of the system with open/periodic boundary condition in x/y directions, and an argument about effects of chiral gapless electronic edge mode on chiral exciton edge modes.

- [64] B. I. Halperin, Phys. Rev. B **25**, 2185 (1982).
- [65] Y. Hatsugai, Phys. Rev. Lett. **71**, 3697 (1993).
- [66] T. Giamarchi, *Quantum Physics in One Dimension* (Clarendon Press, Oxford 2006). Chap. 10, p. 328
- [67] A. A. Serga, T. Schneider, B. Hillebrands, S. O. Demokritov, and M. P. Kostylev, Applied Physics Letters, **89**, 063506 (2006).
- [68] T. Schneider, A. A. Serga, T. Neumann, B. Hillebrands, and M. P. Kostylev, Phys. Rev. B **77**, 214411 (2008).
- [69] S. O. Demokritov, and B. Hillebrands, and A. N. Slavin, Physics Reports, **348**, 441 (2001).
- [70] H. H. Kung, S. Maiti, X. Wang, S. W. Cheong, D. L. Maslov, and G. Blumberg, arxiv:1706.05776v2
- [71] R. Yu et al., Science **329**, 61 (2010).
- [72] Z. Wang, C. Tang, R. Sachs, Y. Barlas, and J. Shi, Phys. Rev. Lett. **114**, 016603 (2015).

Supplemental Material

EFFECTIVE HAMILTONIANS FOR EXCITON BAND TOUCHINGS

Γ and P Points

Effective Hamiltonians for the exciton band touchings at high symmetric points can be derived from a symmetry analysis on an effective equation of motion for a single exciton (BS equation) [1, 2]. We begin with an exciton creation operator:

$$b_{a,\mathbf{k}}^\dagger \equiv \sum_{\mathbf{q}} \phi_a(\mathbf{q}, \mathbf{k}) f_{\mathbf{q}+\frac{\mathbf{k}}{2},c}^\dagger f_{\mathbf{q}-\frac{\mathbf{k}}{2},v} \quad (9)$$

where $f_{\mathbf{q},j}^\dagger$ denotes a creation operator for conduction band electron ($j = c$) or valence band electron ($j = v$). $\phi_a(\mathbf{q}, \mathbf{k})$ is an eigen wavefunction of the Bethe-Salpeter equation. For Eqs. (1,2) in the main text, the eigenvalue problem takes a form of

$$\begin{aligned} \sum_{\mathbf{q}'} K(\mathbf{q}, \mathbf{q}'; \mathbf{k}) \phi_a(\mathbf{q}', \mathbf{k}) &= E_{a,\mathbf{k}} \phi_a(\mathbf{q}, \mathbf{k}), \quad (10) \\ K(\mathbf{q}, \mathbf{q}'; \mathbf{k}) &= \delta_{\mathbf{q},\mathbf{q}'} (\mathcal{E}_{\mathbf{q}+\mathbf{k}/2,c} - \mathcal{E}_{\mathbf{q}-\mathbf{k}/2,v}) \\ &+ \frac{U}{N^2} \langle \mathbf{q} + \frac{\mathbf{k}}{2}, c | \mathbf{q} - \frac{\mathbf{k}}{2}, v \rangle \langle \mathbf{q}' - \frac{\mathbf{k}}{2}, v | \mathbf{q}' + \frac{\mathbf{k}}{2}, c \rangle \\ &- \frac{U}{N^2} \langle \mathbf{q} + \frac{\mathbf{k}}{2}, c | \mathbf{q}' + \frac{\mathbf{k}}{2}, c \rangle \langle \mathbf{q}' - \frac{\mathbf{k}}{2}, v | \mathbf{q} - \frac{\mathbf{k}}{2}, v \rangle. \quad (11) \end{aligned}$$

Here $|\mathbf{q}, j\rangle$ and $\mathcal{E}_{\mathbf{q},j}$ are an eigenvector and eigenvalue of the non-interacting Hamiltonian $\mathbf{H}_{sp}(\mathbf{q})$. The Hamiltonian is symmetric under a magnetic point group $4m'm' = \{E, C_4, C_4^2, C_4^{-1}, \sigma_x T, \sigma_y T, \sigma_X T, \sigma_Y T\}$, with a 4-fold rotation around z -axis C_4 , a mirror with respect to μz plane σ_μ and time-reversal T . Since the interaction part respects the symmetry, the BS Hamiltonian $K(\mathbf{q}, \mathbf{q}'; \mathbf{k})$ is also symmetric under $4m'm'$, e.g.,

$$\begin{aligned} K(\mathbf{q}, \mathbf{q}'; \mathbf{k}) &= K(C_4(\mathbf{q}), C_4(\mathbf{q}'); C_4(\mathbf{k})), \\ K^*(\mathbf{q}, \mathbf{q}'; \mathbf{k}) &= K(-\sigma_x(\mathbf{q}), -\sigma_x(\mathbf{q}'); -\sigma_x(\mathbf{k})). \end{aligned}$$

Eigen wavefunctions of the BS Hamiltonian at Γ and P points form an irreducible corepresentation (IcREP) of $4m'm'$. There are four distinct 1-dimensional IcREPs of $4m'm'$. They are A , B , E_1 , and E_2 [3], in which the eigen wavefunction $\phi_a(\mathbf{q}, \mathbf{k})$ is transformed with s , d , $p_x + ip_y$ and $p_x - ip_y$ -wave symmetry under the symmetry operation on \mathbf{q} (and \mathbf{k}) respectively (see Table I), e.g.,

$$\begin{aligned} \phi_{E_1}(C_4^{-1}(\mathbf{q}), \mathbf{k} = 0) &= (+i)\phi_{E_1}(\mathbf{q}, \mathbf{k} = 0), \\ \phi_{E_1}^*(-\sigma_X(\mathbf{q}), \mathbf{k} = 0) &= (+i)\phi_{E_1}(\mathbf{q}, \mathbf{k} = 0). \end{aligned}$$

The exciton band touchings at the highest symmetric points are composed by those two eigen wavefunctions belonging to distinct IcREPs: any level crossings between

TABLE I. character table of $4m'm'$

	E	C_4^1	C_4^2	C_4^{-1}	$\sigma_x T$	$\sigma_y T$	$\sigma_X T$	$\sigma_Y T$
A	1	1	1	1	1	1	1	1
B	1	-1	1	-1	1	1	-1	-1
E_1	1	+i	-1	-i	1	-1	+i	-i
E_2	1	-i	-1	+i	1	-1	-i	+i

two eigenstates that belong to a same IcREP are generally lifted by symmetry-allowed terms, thus they are not stable band touchings.

A form of the effective 2×2 Hamiltonian formed by a pair of two distinct IcREPs is determined by the symmetry. As an example, consider that E_1 (p_+) and E_2 (p_-) states form a band touching at Γ point and $X_m = 0$ (X_m is a model parameter such as m and t in Fig. 3 in the main text). By the $\mathbf{k} \cdot \mathbf{p}$ perturbation theory, the BS Hamiltonian gives out a 2×2 effective Hamiltonian around this degeneracy point:

$$[\mathbf{H}_{\text{eff}}^{2 \times 2}(\mathbf{k}, X_m)]_{i,j} \equiv \sum_{\mathbf{q}, \mathbf{q}'} \phi_i^{0*}(\mathbf{q}) K(\mathbf{q}, \mathbf{q}'; \mathbf{k}, X_m) \phi_j^0(\mathbf{q}'), \quad (12)$$

($i, j = E_1, E_2$). Here $\phi_j^0(\mathbf{q})$ is an eigenstate of the BS Hamiltonian at $\mathbf{k} = 0$ and $X_m = 0$:

$$\sum_{\mathbf{q}'} K(\mathbf{q}, \mathbf{q}'; \mathbf{k} = 0, X_m = 0) \phi_j^0(\mathbf{q}') = E_0 \phi_j^0(\mathbf{q})$$

with $j = E_1, E_2$. From the Hellmann-Feynman theorem, the effective Hamiltonian at $\mathbf{k} = 0$ with small X_m is diagonal:

$$\mathbf{H}_{\text{eff}}^{2 \times 2}(\mathbf{k}, X_m) = (E_0 + a_+ X_m) \boldsymbol{\tau}_0 + a_- X_m \boldsymbol{\tau}_3 + \mathcal{O}(X_m^2), \quad (13)$$

with $2a_\pm = a_{E_1} \pm a_{E_2}$ and $a_j \equiv \langle \phi_j^0 | (\partial_{X_m} K) |_{X_m=0} | \phi_j^0 \rangle$. The \mathbf{k} -dependence of the Hamiltonian is constrained by the symmetries of E_1 and E_2 states (Table I),

$$\begin{aligned} \mathbf{H}_{\text{eff}}^{2 \times 2*}(-\sigma_X(\mathbf{k}), X_m) &= \mathbf{H}_{\text{eff}}^{2 \times 2*}(-\sigma_Y(\mathbf{k}), X_m) \\ &= \mathbf{H}_{\text{eff}}^{2 \times 2}(C_4^\pm(\mathbf{k}), X_m) = \boldsymbol{\tau}_3 \mathbf{H}_{\text{eff}}^{2 \times 2}(\mathbf{k}, X_m) \boldsymbol{\tau}_3, \quad (14) \end{aligned}$$

and

$$\begin{aligned} \mathbf{H}_{\text{eff}}^{2 \times 2*}(-\sigma_{x(y)}(\mathbf{k}), X_m) &= \mathbf{H}_{\text{eff}}^{2 \times 2}(C_4^2(\mathbf{k}), X_m) \\ &= \mathbf{H}_{\text{eff}}^{2 \times 2}(\mathbf{k}, X_m). \quad (15) \end{aligned}$$

These relations in combination with Eq. (13) lead to

$$\begin{aligned} \mathbf{H}_{\text{eff}}^{2 \times 2}(\mathbf{k}, X_m) &= (E_0 + a_+ X_m + a_0 k^2) \boldsymbol{\tau}_0 + a_- X_m \boldsymbol{\tau}_3 \\ &+ a_1 (k_x^2 - k_y^2) \boldsymbol{\tau}_1 + a_2 k_x k_y \boldsymbol{\tau}_2 \\ &+ a_3 k^2 \boldsymbol{\tau}_3 + \mathcal{O}(X_m^2, \mathbf{k}^3). \quad (16) \end{aligned}$$

The same form also applies to the quadratic band touching formed by A (s) and B (d) states. One can have another symmetry-allowed form for exciton band touchings composed by other pairs. For A and E_2 states (and also for E_1 and B states), the band touching takes a form of

$$\mathbf{H}_{\text{eff}}^{2 \times 2}(\mathbf{k}, X_m) = (E_0 + b_+ X_m) \boldsymbol{\tau}_0 + b_- X_m \boldsymbol{\tau}_3 + b k_x \boldsymbol{\tau}_2 + b k_y \boldsymbol{\tau}_1 + \mathcal{O}(X_m^2, \mathbf{k}^2). \quad (17)$$

M point

The effective Hamiltonian for band touching at M points can be derived in the same way. Consider $M = (\pi, 0)$, whose group under which the BS Hamiltonian is invariant at this point is $m'm'2$ (a subgroup of $4m'm'$): $m'm'2 = \{E, C_4^2, \sigma_x T, \sigma_y T\}$. There are two distinct 1-dimensional IcREPs of $m'm'2$ (see Table. II). They are A and B , [3] in which eigenstates of the BS Hamiltonian at $\mathbf{k} = (\pi, 0)$ is transformed with s and p_x -wave symmetry respectively. From the character table, the \mathbf{k} -dependence of the effective Hamiltonian for this band touching is constrained as follows:

$$\begin{aligned} \mathbf{H}_{\text{eff}}^{2 \times 2}(C_2(\mathbf{k})) &= \mathbf{H}_{\text{eff}}^{2 \times 2*}(-\sigma_y(\mathbf{k})) = \boldsymbol{\tau}_3 \mathbf{H}_{\text{eff}}^{2 \times 2}(\mathbf{k}) \boldsymbol{\tau}_3, \\ \mathbf{H}_{\text{eff}}^{2 \times 2*}(-\sigma_x(\mathbf{k})) &= \mathbf{H}_{\text{eff}}^{2 \times 2}(\mathbf{k}). \end{aligned}$$

This leads to

$$\mathbf{H}_{\text{eff}}^{2 \times 2}(\mathbf{k}, X_m) = (E_0 + c_+ X_m) \boldsymbol{\tau}_0 + c_- X_m \boldsymbol{\tau}_3 + c_1 k_x \boldsymbol{\tau}_2 + c_2 k_y \boldsymbol{\tau}_1 + \mathcal{O}(X_m^2, \mathbf{k}^2). \quad (18)$$

TABLE II. character table of $m'm'2$

	E	C_4^2	$\sigma_x T$	$\sigma_y T$
A	1	1	1	1
B	1	-1	1	-1

THE RESPONSE FUNCTION FOR THE SYSTEM WITH OPEN BOUNDARY CONDITION

In the region with non-zero Chern integers in Fig. 3 in the main text, we calculate the response function for the system with open/periodic boundary condition in one (x)/the other (y) direction, to enumerate all possible collective excitations including edge and bulk modes. The formulation given below enables us to qualitatively discuss how gapless electronic edge mode affects the exciton edge modes. We begin with the interacting electron Hamiltonian with open boundary condition in x , $\mathcal{H} = \mathcal{H}_0 + \mathcal{V}$ with $\mathcal{H}_0 = \sum_{k_y} \mathbf{c}_{k_y}^\dagger \mathbf{H}_{sp}(k_y) \mathbf{c}_{k_y}$ and

$$\mathcal{V} = \frac{U}{2N} \sum_{k_{1,y}, k_{2,y}, q_y, \alpha, \beta} \sum_{x=1}^N \mathbf{c}_{k_{1,y}+q_y, x, \alpha}^\dagger \mathbf{c}_{k_{2,y}-q_y, x, \beta}^\dagger \mathbf{c}_{k_{2,y}, x, \beta} \mathbf{c}_{k_{1,y}, x, \alpha}.$$

Here $\mathbf{c}_{k_y}^\dagger$ takes a $2N$ -component vector form,

$$\mathbf{c}_{k_y}^\dagger \equiv \left(c_{k_y, N, s\uparrow}^\dagger \quad c_{k_y, N, p\downarrow}^\dagger \quad \cdots \quad c_{k_y, 1, s\uparrow}^\dagger \quad c_{k_y, 1, p\downarrow}^\dagger \right),$$

where

$$c_{k_y, x, \alpha}^\dagger = \frac{1}{\sqrt{N}} \sum_{y=1}^N e^{ik_y y} c_{\mathbf{r}, \alpha}^\dagger, \quad (19)$$

with $\mathbf{r} \equiv (x, y)$, $x = 1, 2, \dots, N$ and $\alpha = s \uparrow, p \downarrow$. $\mathbf{H}_{sp}(k_y)$ is a $2N \times 2N$ Hermitian matrix, which is a Fourier transform of a tight-binding sp model in the real space with open/periodic boundary in x/y direction.

The generalized random phase approximation [4, 5] gives the response function $\chi^R(\mathbf{r}_j, t_j; \mathbf{r}_m, t_m) \equiv -i\theta(t_j - t_m) \langle [\mathcal{O}_H(\mathbf{r}_j, t_j), \mathcal{O}_H(\mathbf{r}_m, t_m)] \rangle$. The Fourier transform of the response function in the y coordinate and time takes a $4N \times 4N$ matrix form,

$$\chi_{ab}^R(x_j, x_m; k_y, \omega) \equiv \int d(t_j - t_m) \int d(y_j - y_m) e^{-ik_y(y_j - y_m) + i\omega(t_j - t_m)} \chi_{ab}^R(\mathbf{r}_j, t_j; \mathbf{r}_m, t_m) = \chi_{ab}^T(x_j, x_m; k_y, i\omega_n = \omega + i\eta)$$

$$\chi_{ab}^T(k_y, i\omega_n) = \boldsymbol{\Pi}_{ab}^U(k_y, i\omega_n) + U \boldsymbol{\Pi}_{a0}^U(k_y, i\omega_n) \left[\mathbf{1}_{N \times N} - U \boldsymbol{\Pi}_{00}^U(k_y, i\omega_n) \right]^{-1} \boldsymbol{\Pi}_{0b}^U(k_y, i\omega_n) \quad (20)$$

$$\boldsymbol{\Pi}^U(k_y, i\omega_n) \equiv \boldsymbol{\Pi}^0(k_y, i\omega_n) \left[\mathbf{1}_{4N \times 4N} + \frac{U}{2} \boldsymbol{\Pi}^0(k_y, i\omega_n) \right]^{-1}, \quad (21)$$

with $N \times N$ matrix $\chi_{ab}^T(k_y, i\omega_n)$ as $[\chi_{ab}^T(k_y, i\omega_n)]_{(x_j, x_m)} \equiv \chi_{ab}^T(x_j, x_m; k_y, i\omega_n)$ ($x_j, x_m = 1, \dots, N$). $N \times N$ matrices

$\mathbf{\Pi}_{ab}^U(k_y, i\omega_n)$ and $\mathbf{\Pi}_{ab}^0(k_y, i\omega_n)$ ($a, b = 0, 1, 2, 3$) comprise $4N \times 4N$ matrices $\mathbf{\Pi}^U(k_y, i\omega_n)$ and $\mathbf{\Pi}^0(k_y, i\omega_n)$ respectively,

$$\begin{aligned} [\mathbf{\Pi}^U(k_y, i\omega_n)]_{(a,b)} &\equiv \mathbf{\Pi}_{ab}^U(k_y, i\omega_n), \\ [\mathbf{\Pi}^0(k_y, i\omega_n)]_{(a,b)} &\equiv \mathbf{\Pi}_{ab}^0(k_y, i\omega_n). \end{aligned}$$

A bare polarization function $\mathbf{\Pi}^0(k_y, i\omega_n)$ is given by single-particle electron eigenstates of $\mathbf{H}_{sp}(k_y)$:

$$\begin{aligned} [\mathbf{\Pi}_{ab}^0(k_y, i\omega_n)]_{(x_j, x_m)} &\equiv \frac{1}{\beta} \frac{1}{N} \sum_{q_y} \sum_{i\epsilon_n} \sum_{t,s} \sum_{\alpha, \beta, \gamma, \delta} [\sigma_a]_{\alpha\beta} [\sigma_b]_{\gamma\delta} \frac{\langle x_j, \beta | k_y + q_y, t \rangle \langle k_y + q_y, t | x_m, \gamma \rangle \langle x_m, \delta | q_y, s \rangle \langle q_y, s | x_j, \alpha \rangle}{i(\epsilon_n + \omega_n) - \mathcal{E}_{k_y+q_y, t} + \mu} \frac{1}{i\epsilon_n - \mathcal{E}_{q_y, s} + \mu} \\ &= \frac{1}{N} \sum_{q_y} \sum_{t,s} \sum_{\alpha, \beta, \gamma, \delta} \frac{n_F(\mathcal{E}_{k_y+q_y, t}) - n_F(\mathcal{E}_{q_y, s})}{-i\omega_n + (\mathcal{E}_{k_y+q_y, t} - \mathcal{E}_{q_y, s})} [\sigma_a]_{\alpha\beta} [\sigma_b]_{\gamma\delta} \\ &\quad \times \langle x_j, \beta | k_y + q_y, t \rangle \langle k_y + q_y, t | x_m, \gamma \rangle \langle x_m, \delta | q_y, s \rangle \langle q_y, s | x_j, \alpha \rangle \end{aligned} \quad (22)$$

$n_F(\mathcal{E})$ denotes the Fermi distribution function. In the following, we assume $T = 0$. $|k_y, t\rangle$ and $\mathcal{E}_{k_y, t}$ are the single-particle eigenstate and eigenenergy of $\mathbf{H}_{sp}(k_y)$. This includes both bulk ($t = b'$) and edge states ($t = e'$).

We decompose the bare polarization function into three parts, depending on whether the polarization is induced by bulk states or edge states:

$$\mathbf{\Pi}^0(k_y, i\omega_n) = \mathbf{\Pi}^{0,(b,b)}(k_y, i\omega_n) + \mathbf{\Pi}^{0,(b,e)}(k_y, i\omega_n) + \mathbf{\Pi}^{0,(e,e)}(k_y, i\omega_n). \quad (23)$$

Namely, in $\mathbf{\Pi}^{0,(b,b)}$, the summations over the single-particle states in Eq. (22) (the summations over ‘ s ’ and ‘ t ’ in Eq. (22)) are over the bulk states. In $\mathbf{\Pi}^{0,(e,e)}$, the summations are only over the edge states. In $\mathbf{\Pi}^{0,(b,e)}$, the summation over the particle states (‘ t ’ in Eq. (22)) is over the bulk (edge) states, if that over the hole states (‘ s ’ in Eq. (22)) is taken over the edge (bulk) states. For given k_y , the number of the bulk states is much larger than that of the edge states. Therefore, $\mathbf{\Pi}^{0,(b,b)}$ has a major contribution to $\mathbf{\Pi}^0$. $\mathbf{\Pi}^{0,(b,e)}$ and $\mathbf{\Pi}^{0,(e,e)}$ have secondary roles, which we will discuss later.

For ω below the electron-hole continuum of the bulk states, $\mathbf{\Pi}^{0,(b,b)}(k_y, \omega)$ is a Hermitian matrix. $\mathbf{\Pi}^U$ (or $\mathbf{\chi}^R$) made only out of such $\mathbf{\Pi}^{0,(b,b)}$ by Eqs. (21,20) can be diagonalized by a unitary matrix, unless one of its eigenvalues has a pole. Namely,

$$[\mathbf{\Pi}^U(k_y, \omega)]^{-1} |v_a(k_y, \omega)\rangle = |v_a(k_y, \omega)\rangle \mathcal{L}_a^D(k_y, \omega) \quad (24)$$

where $|v_a(k_y, \omega)\rangle$ with $a = 1, \dots, 4N$ form an orthonormal basis for those ω with $\mathcal{L}_a^D(k_y, \omega) \neq 0$ for any a . Like in the bulk calculation (see main text), each eigenvalue has at most one pole below the electron-hole continuum of the bulk states. The pole is determined by the zero of the eigenvalue: $\mathcal{L}_a^D(k_y, E_{a,k_y}) = 0$. E_{a,k_y} gives an energy-momentum dispersion of exciton states with a given momentum k_y . Such exciton states include both bulk exciton states and edge exciton states.

Firstly, we confirm that exciton states thus obtained completely reproduce the lowest two exciton bulk bands obtained from the calculation with periodic boundary conditions both in x and y direction (main text). Besides, we observe that, when an indirect band gap opens between the lowest two exciton bulk bands, new exci-

ton states appear inside the gap. Eigenvalues (E_{a,k_y}) for these in-gap exciton states form chiral energy-momentum dispersions as a function of k_y , connecting the two exciton bulk bands (Fig. 1 in the main text). The number of the chiral dispersions inside the gap including its sign turns out to be identical to the Chern integer of the lowest exciton bulk band. The eigen wavefunctions ($|\tilde{v}_a(k_y)\rangle \equiv |v_a(k_y, \omega = E_{a,k_y})\rangle$) which correspond to these in-gap exciton states, are spatially localized at the boundaries, having weight in the pseudospin component of σ_1 and σ_2 (Fig. 5). These observations justify the presence of the chiral exciton edge modes of the topological origin in sp model with short-range Coulomb interaction, which interact with light.

Let us next discuss effects of $\mathbf{\Pi}^{0,(b,e)}$ and $\mathbf{\Pi}^{0,(e,e)}$. The electronic edge mode is gapless, so that these two have both Hermitian and anti-Hermitian parts. Nonetheless, any matrix element of the anti-Hermitian part of $\mathbf{\Pi}^{0,(b,e)}$ is negligibly small in the thermodynamic limit. Namely, the bulk states are extended in space, so that an integrand in Eq. (22) for $\mathbf{\Pi}^{0,(b,e)}$ is at most on the order of $1/N$, i.e.,

$$\begin{aligned} &\langle x_j, \beta | k_y + q_y, t = b \rangle \langle k_y + q_y, t = b | x_m, \gamma \rangle \\ &\quad \times \langle x_m, \delta | q_y, s = e \rangle \langle q_y, s = e | x_j, \alpha \rangle < \mathcal{O}\left(\frac{1}{N}\right). \end{aligned} \quad (25)$$

(‘ $t = b'$ ’ and ‘ $s = e'$ ’ means that the single-particle state for t is from the bulk states and that for s is from the edge state). Meanwhile, matrix elements of an anti-Hermitian part of $\mathbf{\Pi}^{0,(e,e)}$, which are also spatially localized at the boundaries, are on the order of 1.

The effect of $\mathbf{\Pi}^{0,(e,e)}(k_y, \omega)$ is two-folded, depending on an energy region ω . In low-energy region, the Hermi-

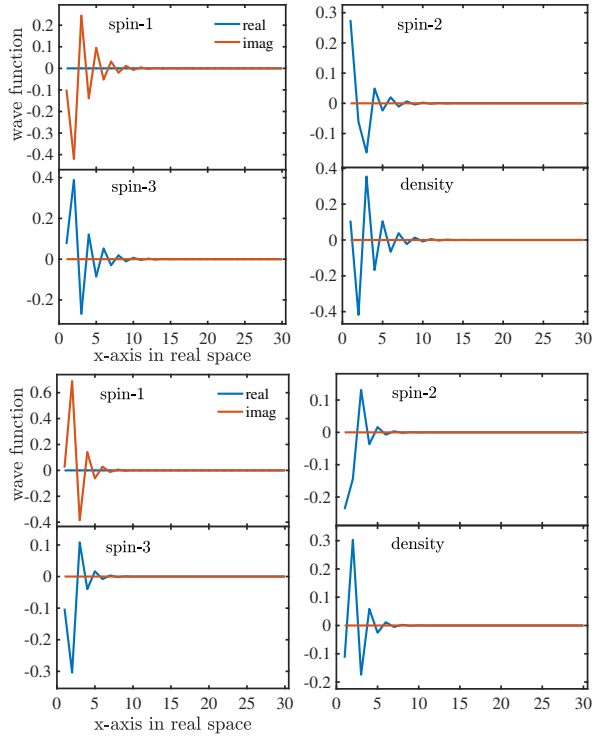


FIG. 5. (color online) Real (blue) and imaginary (red) parts in spin 1 (σ_1), 2 (σ_2), 3 (σ_3) and density (σ_0) components of eigen wavefunctions ($|\tilde{v}_a(k_y)\rangle \equiv |v_a(k_y, E_a, k_y)\rangle$) which correspond to those in-gap exciton states at $k_y = 0.13\pi$ in Fig. 1 in the main text (ingap states with blue color chiral dispersion). They are plotted as a function of the spatial coordinate x . $x = 0$ and $x = 30$ correspond to the left-hand-side and right-hand-side spatial boundary. The upper four are for Fig. 1(a) and the lower four are for Fig. 1(b) in the main text.

tian part of $\Pi^{0,(e,e)}$ leads to the one-dimensional chiral

phason mode. Being a well-defined low-energy collective bosonic excitation, the phason mode has a level crossing (and consequently level repulsion) with low-energy chiral exciton edge modes (Fig. 4 in the main text). The level repulsion changes total number of low-energy chiral dispersions of edge excitons which go across the indirect gap between the lowest two exciton bulk bands. For $0 < m < 2t$ ($-2t < m < 0$), total number of the chiral dispersions becomes $\mathbb{Z} - 1$ ($\mathbb{Z} + 1$) instead of \mathbb{Z} , where \mathbb{Z} is the Chern integer of the lowest bulk exciton band.

In high-energy region, the anti-Hermitian part of $\Pi^{0,(e,e)}$ results in a finite region of an edge electron-hole continuum. The electronic edge mode in the high energy region generally has a curvature in its energy-momentum dispersion. Electron-hole excitations along such electronic edge mode form a finite region of a new electron-hole continuum (below the electron-hole continuum of the bulk states). When the chiral exciton edge modes share energy and momentum with the edge electron-hole continuum, they acquire a finite life time (Fig. 4 in the main text).

* rshindou@pku.edu.cn

- [1] G. E. Pikus and G. L. Bir, Zh. Eksp. Teor. Fiz. **60**, 195 (1971) [Sov. Phys. JETP **33**, 108 (1973)].
- [2] M. Z. Maialle, E. A. de Andrada e Silva, and L. J. Sham, Phys. Rev. B **47**, 15776 (1993).
- [3] C. J. Bradley, and A. P. Cracknell, *The Mathematical Theory of Symmetry in Solids* (The Clarendon Press, Oxford, 1972). Chap. 7, p. 569.
- [4] A. L. Fetter and J. D. Walecka, *Quantum Theory of Many-Particle Systems* (Dover Publications, Mineola, New York, 2003), Chap. 4, p. 128.
- [5] W. Hanke and L. J. Sham, Phys. Rev. B **21**, 4656 (1980).